Time dependence of the thermal-photon thermometer

Fan Zhang,[1,*] Cheng Li,[2,3] Pei-Wei Wen,[4] Jian-Wei Liu,[1] Jun Su,[5] and Feng-Shou Zhang[2,3,6]

[1]*Department of Electronic Information and Physics, Changzhi University, Changzhi 046011, China*

[2]*Beijing Radiation Center, Beijing 100875, China*

[3]*College of Nuclear Science and Technology, Beijing Normal University, 100875 Beijing, China*

[4]*China Institute of Atomic Energy, Beijing 102413, China*

[5]*Sino-French Institute of Nuclear Engineering and Technology Sun Yat-sen University, Zhuhai 519082, China*

[6]*Center of Theoretical Nuclear Physics, National Laboratory of Heavy Ion Accelerator of Lanzhou, Lanzhou 730000, China*

(Received 9 June 2018; revised manuscript received 9 May 2019; published 2 August 2019)

A systematic study of the thermal-photon thermometer is presented for heavy-ion collisions at intermediate energies via the isospin-dependent quantum molecular dynamics model. We find that the duration of the thermal hard photons production is more than 500 fm/c. The divergence between the initial temperature and the final measurement temperature is about 5%. The isospin dependence of the nuclear temperature is consistent between the initial temperature and the final measurement temperature. As a comparison, the slope and double-isotope ratio thermometers are also discussed.

DOI: 10.1103/PhysRevC.100.024603

I. INTRODUCTION

Nucleus-nucleus collisions at intermediate energies aim at the study of the phase diagram of nuclear matter at densities and temperatures where a transition from the Fermi liquid ground state to the nucleon gas phase has been predicted [1].

The determination of the thermodynamical properties such as temperature, density, and excitation energy of the hot nuclear systems produced in nucleus-nucleus reactions is one of the main goals of heavy-ion physics. During the past two decades, many studies were committed to measuring the nuclear temperatures and phase transition in multifragmentation [2–10]. The relation between the temperature and the excitation energy of a system is of fundamental importance in a wide variety of physical systems [11]. In order to determine temperatures of colliding systems, various thermometers have been developed and applied to study the highly excited nuclear systems, such as the slope thermometer (using light particles) [12,13], the isotopic thermometer [14], and the population of excited states thermometer [15,16]. Due to the interaction among the particles, the above thermometers are polluted by the reaction environment. Electromagnetic probes, viz., photons, due to their weak final state interaction with the surrounding medium, have been recognized as the most direct probes of the space-time evolution of the colliding nucleons [17]. Photons produced in heavy-ion (HI) reactions escape freely from the interaction region. The inverse slope parameter of their spectrum E_0^t and the temperature T of the nuclear medium are strongly correlated [18]. Martínez has suggested that the thermal hard photons are emitted from a nearly thermalized source and still originate from bremsstrahlung produced in p-n collisions [19]. By applying the bremsstrahlung photons in multifragment ^{36}Ar + ^{197}Au reactions, d'Enterria *et al.* have shown the evidence for thermal equilibration in multifragmentation reactions [20].

Using the bremsstrahlung photons, the nuclear temperature can be determined by measuring the slope of the reaction's thermal hard-photon spectrum [18]. However, the thermal hard photons are produced during a period of time. At moderate excitation energies, $\epsilon^* \approx 3A$–$10A$ MeV, the time of thermal hard-photon production is about 200 fm/c or even more longer [18,19]. During this time, the thermodynamical properties of the hot nucleus will be changed. Naturally, one may think about how the deexcitation process influences the slope of the hard-photon spectrum and the measurement of temperature.

II. MODEL AND METHODS

In this work, we attempt to study the time dependence of the thermal-photon thermometer, within the isospin-dependent quantum molecular dynamics (IQMD) model [21,22]. In the present model, the Hamiltonian H is expressed as

$$H = \tau + U_{\rm Coul} + \int V(\rho) dr, \tag{1}$$

where τ is the kinetic energy and $U_{\rm Coul}$ is the Coulomb potential energy. $V(\rho)$ is the nuclear potential energy density functional, which is written as

$$V(\rho) = \frac{\alpha}{2}\frac{\rho^2}{\rho_0} + \frac{\beta}{\gamma+1}\frac{\rho^{\gamma+1}}{\rho_0^{\gamma}} + \frac{g_{\rm sur}^{\rm iso}}{2}\frac{(\nabla\rho_n - \nabla\rho_p)^2}{\rho_0} + \frac{g_{\rm sur}}{2}\frac{(\nabla\rho)^2}{\rho_0} + g_\tau\frac{\rho^{8/3}}{\rho_0^{5/3}} + \frac{C}{2}\frac{(\rho_n-\rho_p)^2}{\rho_0}. \tag{2}$$

We use three sets of parameters, as shown in Table I.

The excitation energy E^* of the hot nuclei is calculated by

$$E^* = \tau + V - B, \tag{3}$$

*Corresponding author: zhangfan@mail.bnu.edu.cn

TABLE I. The parameters adopted in the present work.

	α (MeV)	β (MeV)	γ	$g_{\rm sur}$ (MeV fm^5)	$g_{\rm sur}^{\rm iso}$ (MeV fm^5)	C (MeV)	g_τ (MeV)	ρ_0 (fm^{-3})	K (MeV)
Skx [23]	−168.40	115.90	1.50	92.13	−6.97	38.13	0.40	0.16	271
Soft [21]	−356.00	303.00	1.17	130.00	0.00	39.40	0.00	0.16	200
Hard [21]	−124.00	70.5.0	2.00	130.00	0.00	39.40	0.00	0.16	380

where τ and V are kinetic energy and potential energy of the hot nuclei. B is the binding energy of the hot nuclei at the ground state.

We perform a systematic study of the hot nuclei in a wide excitation energy range and a wide asymmetry range. A hot nucleus could be produced in central heavy-ion collisions at intermediate energies. Calculations predict that at higher bombarding energies (approximately larger than 100 MeV/nucleon) the expansion is sufficiently violent to break up the system into many fragments, and no thermal hard photons are produced [19]. In this work, the hard photon production with small mass projectile and large mass target, such as ^{36}Ar + ^{190}W, has been studied. In such systems there are enough nucleons in the overlap volume of target and projectile to experience more than the minimal 20–30 collisions needed for thermalization to take place.

The asymmetry of the hot nuclei is defined as

$$m_s = \frac{N_s - Z_s}{A_s}, \tag{4}$$

where N_s, Z_s, and A_s are the neutron number, proton number, and mass number of the hot nuclei. Using the hot nuclei, we could study the time dependence of the thermal hard-photon spectrum. A measure of the equilibration is given by the quadrupole moment of the momentum distribution,

$$Q_p = \int \left(2p_z^2 - p_x^2 - p_y^2\right) f(\mathbf{r}, \mathbf{p}, t) d\mathbf{r}\, d\mathbf{p}. \tag{5}$$

In this work we use the one-boson-exchange model by Gan *et al.* to evaluate the elementary $pn \to pn\gamma$ probability [24]. The single differential probability is

$$p_\gamma \equiv \frac{dN}{d\varepsilon_\gamma} = 2.1 \times 10^{-6} \frac{(1-y^2)^\alpha}{y}, \tag{6}$$

where $y = \varepsilon_\gamma / E_{\rm max}$, $\alpha = 0.7319 - 0.5898\beta_i$, and β_i and $E_{\rm max}$ are the initial velocities of the proton and the energy available in the center of mass of the colliding proton-neutron pairs. The hard-photon spectra can be described by the sum of two exponential distributions characterized by inverse slopes E_0^d and E_0^t, corresponding to a direct and a thermal component, respectively, with their corresponding weights:

$$\frac{d\sigma}{dE_\gamma} = K_d e^{-E_\gamma/E_0^d} + K_t e^{-E_\gamma/E_0^t}. \tag{7}$$

[19,20]. The temperature T of the emitting sources and the photon slope parameter E_0^t are found to be well described by the relation

$$T\ ({\rm MeV}) = (0.78 \pm 0.02) \times E_0^t\ ({\rm MeV}), \tag{8}$$

in the range $T \approx$ 3–10 MeV [18].

III. RESULTS AND DISCUSSION

In the IQMD model, the temporal evolutions of baryons in the system are governed by Hamiltonian equations of motion. The distributions of nucleons determine density fluctuation. The distributions of nucleons are determined by kinetic energy of nucleons, mean field (the density function simulates the short-range attractive nuclear forces), and nucleon-nucleon (NN) collisions (collisions simulate the short-range repulsive nuclear forces). In heavy ion collisions, nucleons will have local collective kinetic energy through nucleon-nucleon collisions and the mean field. If some nucleons move away from other nucleons, their collective kinetic energy is large enough and cannot be dissipated by mean field. The distance between these nucleons and other nucleons will increase. The distributions of nucleons become nonuniform. Density fluctuation becomes larger. If their distance becomes longer, they no longer interact with each other because the nuclear forces are of short range. Clusters can be formed.

Figure 1 shows the density distribution for the system ^{36}Ar + ^{190}W at 60 MeV/nucleon in the x-z plane and central collisions. In the first stage of the collision a dense system is formed which then slowly expands until the attractive part of nuclear force is strong enough to drive a second compression of the system. Around $t = 50$ fm/c the first maximum overlap of the two nuclei is achieved. The system subsequently undergoes oscillations around the saturation density, and a hot nucleus is formed. We can see that one oscillation is about 100 fm/c.

In order to select the nucleons which are part of a hot nucleus, nucleons with relative distance $R \leqslant 3$ fm are coalesced into a group (a cluster). This value corresponds to the typical

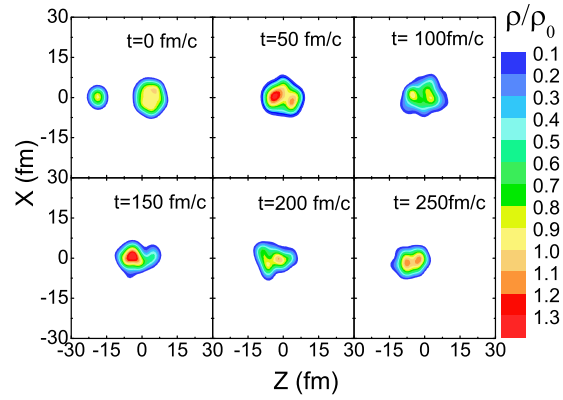

FIG. 1. Density contours in ^{36}Ar + ^{190}W collisions at impact parameter $b = 0$ fm and beam energy 60 MeV/nucleon, calculated with nuclear force parameters Skx.

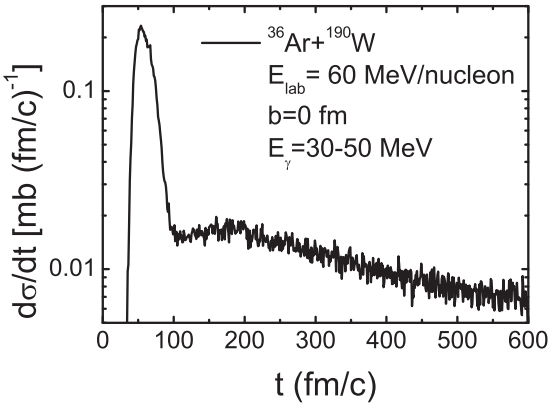

FIG. 2. Production rate of photons with energy 30–50 MeV for the maximum mass cluster, calculated with nuclear force parameters Skx.

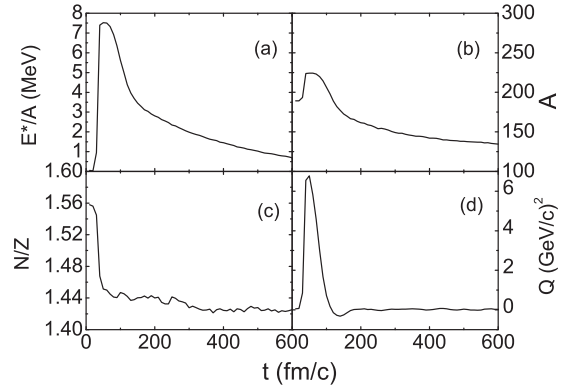

FIG. 3. Time evolution of the excitation energy (a), mass (b), neutron-to-proton ration (N/Z) (c), and quadrupole moment (d) for the maximum mass cluster in central $^{36}\mathrm{Ar} + {}^{190}\mathrm{W}$ collision at 60 MeV/nucleon, calculated with nuclear force parameters Skx.

range of the nuclear force. In this work, we only study the dynamical evolution of the hot nuclei. If one wants to study the final fragment production, a dynamical model incorporating the statistical decay model should be used [25–27]. The dynamical evolution is simulated by the IQMD model. The statistical decay model is used to calculate the decay of primary fragments. The primary fragments are recognized by a minimum spanning tree algorithm, in which nucleons with relative distance of coordinate and momentum of $|r_i - r_j| \leqslant R$ and $|p_i - p_j| \leqslant P$ belong to a fragment. The parameters $R = 3$ fm and $P = 250$ MeV/c are chosen. After the evolution by the IQMD code, the hot fragments are formed, and the statistical decay model is switched on.

The computed production rates of hard photons with energy of 30–50 MeV are shown as a function of the reaction time in Fig. 2. They were calculated for the system $^{36}\mathrm{Ar} + {}^{190}\mathrm{W}$ at 60 MeV/nucleon bombarding energy and central collision. There are two distinct hard-photon sources clearly separated in time because of the absence of photon production during the expansion phase. The figure indicates also a radical difference in the energy spectra of photons from the two sources, thermal hard photons having a softer spectrum than direct ones. In the first stage ($t < 110$ fm/c), the hot nuclear system is not equilibrated [see the quadrupole moment in Fig. 3(d)]. During this stage the hard photons are produced via first-chance collisions. After this stage hard photons are produced in an approximately equilibrated thermal source [cf. Fig. 3(d)], but their production rate is small compared with that of the first-chance collisions. When the system is almost fully thermalized, a hot nucleus is formed. The photons originating from this source are called thermal hard photons [19]. Since the hot nucleus is formed around 110 fm/c, the hot nuclei which are used to study the nuclear temperature are selected between 110 and 120 fm/c. The computed production rates of thermal hard photons decrease with increasing time, but the duration of the thermal hard photons production is more than 500 fm/c.

Figure 3 shows the time evolution of mass, excitation energy, neutron-to-proton ratio N/Z, and quadrupole moment for the maximum mass cluster. They were calculated for the system $^{36}\mathrm{Ar} + {}^{190}\mathrm{W}$ at 60 MeV/nucleon bombarding energies and at an impact parameter of $b = 0$ fm. The quadrupole moment in momentum space [Fig. 3(d)] is defined by Eq. (5), which indicates the equilibration of the momentum distribution. We can see that the quadrupole moment reaches $Q_p \approx 0$ around 110 fm/c, which reflects that the maximum mass cluster approximately reaches a global thermodynamical equilibrium.

It is clear that the mass and excitation energy of the maximum mass cluster decrease with increasing reaction time. Due to the deexcitation of the maximum mass cluster, the excitation energy decreases from 5 to 1 MeV for a time period of 500 fm/c. The mass number of the maximum mass cluster decreases from 200 to 140. The mass number decrease quickly before 150 fm/c, which is consistent with usual estimates of the first breakup time interval $\tau_0 \approx 100$ fm/c [28]. Due to the preequilibrium emission, the N/Z of the maximum mass cluster is around 1.43 and almost constant, which is smaller than the N/Z of the reaction system (1.46).

In order to further study the degree of thermalization, we check stopping. Bauer predicted that the degree of stopping could be a sensitive observable to check the nuclear equilibration [29]. To analyze the nonequilibrium dynamics, we investigate the time evolution of several observables for the maximum mass cluster in Fig. 4. Figure 4(a) shows the time evolutions of potential energy and the number of NN collisions in central $^{36}\mathrm{Ar} + {}^{190}\mathrm{W}$ collisions at 60 MeV/nucleon. The evolution of the potential energy can describe the global compression and expansion. The compression of the system is much smaller than the expansion of the system ($t <$ 100 fm/c). Thus, the NN collisions are responsible for the beam energy dissipation. Figure 4(b) shows the time evolution of stopping. To quantify the degree of stopping, one adopts the ratio of transverse to parallel quantities, R_E [30]. The stopping of the maximum mass cluster is around 1 before collision ($t <$ 30 fm/c). When target and projectile are in contact ($t \approx 30$ fm/c), the stopping decreases rapidly. With the increase of NN collisions, the beam energy is dissipated. The longitudinal energy is transferred to transversal energy. The stopping increases visibly in the period 30 to 110 fm/c in Fig. 4(b), when the number of NN collisions is large. Since the stopping

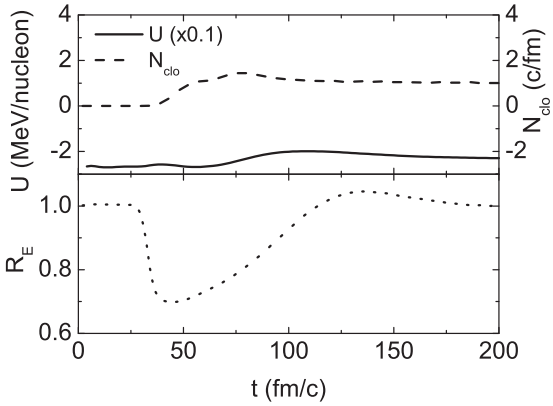

FIG. 4. (a) Time evolutions of the potential energy and the number of nucleon-nucleon collisions for the maximum mass cluster. (b) Time evolution of stopping for the maximum mass cluster, calculated with nuclear force parameters Skx.

reaches the value of 1 around 110 fm/c, the global equilibrium is achieved. After 110 fm/c, the number of NN collisions is about 1 c/fm. NN collisions are thermal collisions. We can also see that there is a weak compression which is caused by the mean field on the maximum mass cluster.

Figure 5 shows the thermal hard-photon slope E_0^t as a function of the (Coulomb-corrected) nucleus-nucleus center-of-mass energy. The behavior of the calculated hard-photon spectra slope E_0^t is generally in agreement with the data.

Applying Eq. (8), the nuclear temperature attained in a HI reaction can be determined by measuring the slope of its thermal hard-photon spectrum. In order to decrease the mass effect on the nuclear temperatures, the masses of the hot nuclei are required to be $190 \leqslant A \leqslant 200$ or $165 \leqslant A \leqslant 175$, satisfying the requirements. For Skx and soft parameters, the mass is required to be $190 \leqslant A \leqslant 200$. For hard parameters, the mass is required to be $165 \leqslant A \leqslant 175$. To further investigate the time dependence of nuclear temperatures at different excitation energies, we display the initial temperatures and the

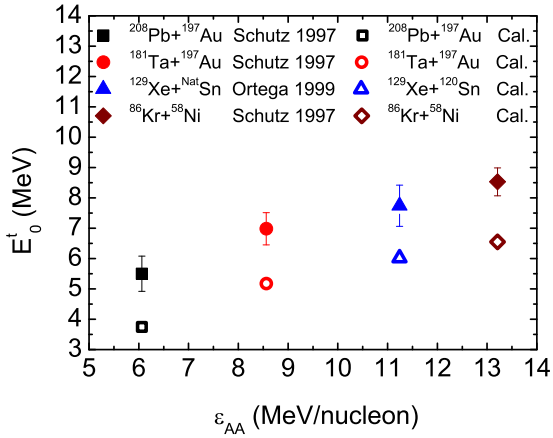

FIG. 5. Thermal hard-photon slope E_0^t as a function of the (Coulomb-corrected) nucleus-nucleus center-of-mass energy, ϵ_{AA}, calculated with nuclear force parameters Skx. Experimental data are taken from Schutz [31] and Ortega [32].

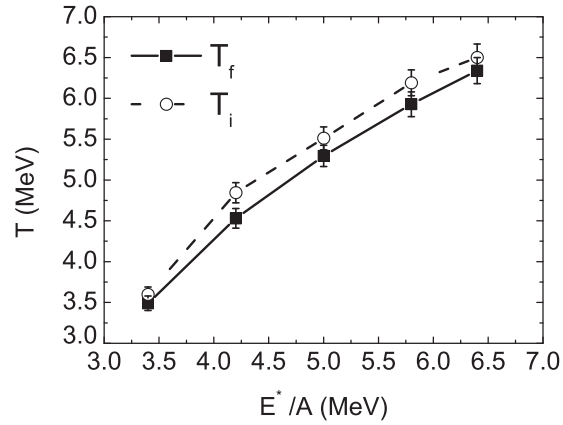

FIG. 6. The temperatures for initial temperature (open shape) and final measurement temperature (full shape) extracted with the thermal-photon thermometer. In the calculation, the Skx parameters are used.

final measurement temperatures as a function of excitation energy in Fig. 6. In this paper, we define the temperature calculated by emission particles and hard photons before 150 fm/c as the initial temperature T_i, and emission particles and hard photons before 600 fm/c as the final measurement temperature T_f. The thermal hard photons are produced in the reactions of ^{36}Ar $+^{168}$ Er at 30 MeV/nucleon, ^{36}Ar $+^{176}$ Lu at 40 MeV/nucleon, ^{36}Ar $+$ ^{197}Au at 60 MeV/nucleon, and ^{36}Ar $+^{206}$ Bi at 95 MeV/nucleon at an impact parameter of $b = 0$ fm.

It can be seen from Fig. 6 that T_i is greater than T_f. This is mainly because of the evaporation of the hot nuclei. As a result the excitation energy is slowly cooling down. Thus the temperature will also decrease. The divergence of the temperature T between T_f and T_i is about 5% across all E^*/A.

To examine in more detail the temperature shift of the emission time with the changing source asymmetry, we plot caloric curves for different time ranges in Fig. 7. The hard

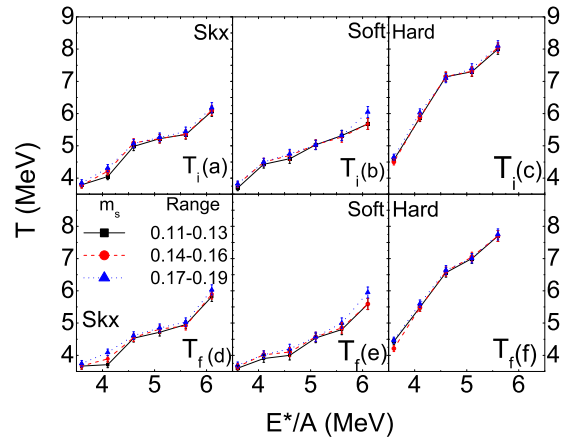

FIG. 7. Caloric curves for the hot nuclei, extracted with the thermal-photon thermometer. The different curves correspond to narrow selections on the source asymmetry for the initial temperature (a)–(c) and final measurement temperature (d)–(f). In the calculation, the Skx, soft, and hard parameters are used.

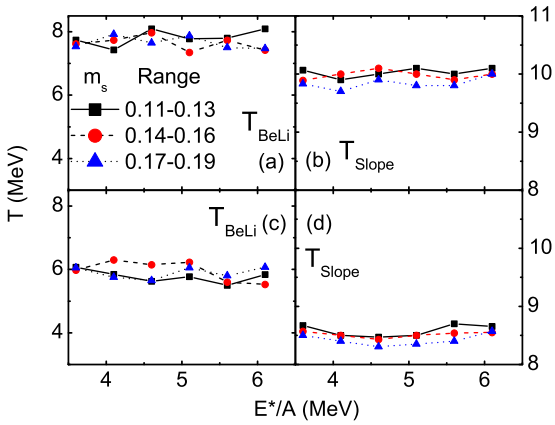

FIG. 8. Caloric curves for the hot nuclei with mass $190 \leqslant A \leqslant 200$, extracted with the slope and double-isotope ratio thermometers. The different curves correspond to narrow selections on the source asymmetry for the initial temperature (a)–(b) and final measurement temperature (c)–(d), calculated with nuclear force parameters Skx.

photons in $^{36}\mathrm{Ar} + ^{171}\mathrm{Yb}$, $^{173}\mathrm{Ta}$, and $^{173}\mathrm{Er}$ at 35 and 40 MeV/nucleon, $^{36}\mathrm{Ar} + ^{187}\mathrm{Au}$, $^{188}\mathrm{Os}$, and $^{190}\mathrm{W}$ at 55, 60, and 65 MeV/nucleon, and $^{36}\mathrm{Ar} + ^{206}\mathrm{Bi}$, $^{206}\mathrm{Rn}$, and $^{204}\mathrm{Hg}$ at 95 MeV/nucleon have been studied. In Figs. 7(a)–7(c), the caloric curves were obtained with the thermal-photon thermometer using early emitted photons, calculated with the Skx, soft, and hard parameters. It is clear that the temperatures for the neutron-rich hot nuclei are higher. In Figs. 7(d)–7(f), the caloric curves are obtained using the emitted photons, which are emitted over a range of times. We can see that the isospin dependence of the nuclear temperatures is consistent between T_i and T_f for different parameters.

Since there was usually inconsistency between kinematic and double-isotope ratio temperatures, we also compare the slope and double-isotope ratio temperatures in Fig. 8. The double-isotope ratio temperatures T_{BeLi} are shown in Figs. 8(a) and 8(c). Here, the double-isotope ratio temperature is calculated as $T_{\mathrm{BeLi}} = (11.3\ \mathrm{MeV})/\ln(1.8\frac{Y(^9\mathrm{Be})/Y(^8\mathrm{Li})}{Y(^7\mathrm{Be})/Y(^6\mathrm{Li})})$. For comparison, the slope temperatures (T_{slope}) for protons are shown in Figs. 8(b) and 8(d). The double-isotope ratio thermometer is used to calculate the freeze-out temperature and cannot be used to study the initial temperature of the hot nuclei. Thus, the initial temperatures T_i of the double-isotope ratioonly are used to compare with T_f. Using the double-isotope ratio thermometer, the nuclear temperatures show almost no isospin effect. However, using the slope thermometer the nuclear temperatures are higher for neutron-poor systems. The isospin dependence of the nuclear temperatures is consistent between T_i and T_f. Since the three thermometers to be employed operate in fundamentally different ways, for the slope thermometer the value of the temperature is extracted from the slope of the kinetic energy spectra. The kinematic characteristics reflect not only the thermal properties of the system but also the Fermi motion at freeze-out, collective effects, and recoil effects [24]. The double-isotope ratio thermometer will be affected by secondary decay. Therefore, the difference of the isospin effect between different thermometers should be further discussed in the future.

IV. CONCLUSIONS

In summary, we have presented a study about the time dependence of the thermal-photon thermometer using the IQMD model. The duration of the thermal hard photons production is more than 500 fm/c. Due to the deexcitation and fragmentation of the hot nuclei, the excitation energy and mass of systems are changed. The divergence of the temperature T between the initial temperature T_i and the final measured temperature T_f was obtained using the thermal hard photons. We find that the divergence between the T_i and T_f is about 5%. The isospin dependence of the nuclear temperature is consistent between the T_i and T_f.

ACKNOWLEDGMENTS

This work was supported by the National Natural Science Foundation of China under Grants No. 11847036 and No. 11635003, and by the project funded by the China Postdoctoral Science Foundation under Grants No. 2017M621035 and No. 2016M600956.

[1] J. Pochodzlla, Prog. Part. Nucl. Phys. **39**, 443 (1997).
[2] A. Kelić, J. B. Natowitz, and K.-H. Schmidt, Eur. Phys. J. A **30**, 203 (2006).
[3] J. B. Natowitz, R. Wada, K. Hagel, T. Keutgen, M. Murray, A. Makeev, L. Qin, P. Smith, and C. Hamilton, Phys. Rev. C **65**, 034618 (2002).
[4] W. Trautmann *et al.*, Int. J. Mod. Phys. E **17**, 1838 (2008).
[5] C. Sfienti, P. Adrich, T. Aumann, C. O. Bacri, T. Barczyk, R. Bassini, S. Bianchin, C. Boiano, A. S. Botvina, A. Boudard, J. Brzychczyk, A. Chbihi, J. Cibor, B. Czech, M. De Napoli, J.-É. Ducret, H. Emling, J. D. Frankland, M. Hellström, D. Henzlova, G. Immè, I. Iori, H. Johansson, K. Kezzar, A. Lafriakh, A. Le Fèvre, E. Le Gentil, Y. Leifels, J. Lühning, J. Łukasik, W. G. Lynch, U. Lynen, Z. Majka, M. Mocko, W. F. J. Müller, A. Mykulyak, H. Orth, A. N. Otte, R. Palit, P. Pawłowski, A. Pullia, G. Raciti, E. Rapisarda, H. Sann, C. Schwarz, H. Simon, K. Sümmerer, W. Trautmann, M. B. Tsang, G. Verde, C. Volant, M. Wallace, H. Weick, J. Wiechula, A. Wieloch, and B. Zwiegliński, Phys. Rev. Lett. **102**, 152701 (2009).
[6] R. Ogul, A. S. Botvina, U. Atav, N. Buyukcizmeci, I. N. Mishustin, P. Adrich, T. Aumann, C. O. Bacri, T. Barczyk, R. Bassini, S. Bianchin, C. Boiano, A. Boudard, J. Brzychczyk, A. Chbihi, J. Cibor, B. Czech, M. De Napoli, J.-É. Ducret, H. Emling, J. D. Frankland, M. Hellström, D. Henzlova, G. Immè, I. Iori, H. Johansson, K. Kezzar, A. Lafriakh, A. Le Fèvre, E. Le Gentil, Y. Leifels, J. Lühning, J. Łukasik, W. G. Lynch, U. Lynen, Z. Majka, M. Mocko, W. F. J. Müller, A. Mykulyak, H. Orth, A. N. Otte, R. Palit, P. Pawłowski, A. Pullia, G. Raciti,

E. Rapisarda, H. Sann, C. Schwarz, C. Sfienti, H. Simon, K. Sümmerer, W. Trautmann, M. B. Tsang, G. Verde, C. Volant, M. Wallace, H. Wallace, H. Weick, J. Wiechula, A. Wieloch, and B. Zwiegliński, Phys. Rev. C **83**, 024608 (2011).
[7] S. Pal, Phys. Rev. C **81**, 051601(R) (2010).
[8] C. L. Zhou, Y. G. Ma, D. Q. Fang, and G. Q. Zhang, Phys. Rev. C **88**, 024604 (2013).
[9] D. Q. Fang, Y. G. Ma, and C. L. Zhou, Phys. Rev. C **89**, 047601 (2014).
[10] F. Zhang, C. Li, P. W. Wen, H. Liu, and F. S. Zhang, Eur. Phys. J. A **52**, 281 (2016).
[11] A. B. McIntosh, A. Bonasera, P. Cammarata, K. Hagel, L. Heilborn, Z. Kohley, J. Mabiala, L. W. May, P. Marini, A. Raphelt, G. A. Souliotis, S. Wuenschel, A. Zarrella, and S. J. Yennello, Phys. Lett. B **719**, 337 (2013).
[12] G. D. Westfall, Phys. Lett. B **116**, 118 (1982).
[13] B. V. Jacak, G. D. Westfall, C. K. Gelbke, L. H. Harwood, W. G. Lynch, D. K. Scott, H. Stöcker, M. B. Tsang, and T. J. M. Symons, Phys. Rev. Lett. **51**, 1846 (1983).
[14] S. Albergo, S. Costa, E. Costanzo, and A. Rubbion, Nuovo Cimento A **89**, 1 (1985).
[15] D. J. Morrissey, W. Benenson, E. Kashy, B. Sherrill, A. D. Panagiotou, R. A. Blue, R. M. Ronningen, J. vander Plicht, and H. Utsunomiya, Phys. Lett. B **148**, 423 (1984).
[16] J. Pochodzalla, W. A. Friedman, C. K. Gelbke, W. G. Lynch, M. Maier, D. Ardouin, H. Delagrange, H. Doubre, C. Grégoire, A. Kyanowski, W. Mittig, A. Péghaire, J. Péter, F. Saint-Laurent, Y. P. Viyogi, B. Zwieglinski, G. Bizard, F. Lefèbvres, B. Tamain, and J. Québert, Phys. Rev. Lett. **55**, 177 (1985).
[17] W. Cassing, V. Metag, U. Mosel, and K. Niita, Phys. Rep. **188**, 363 (1990).
[18] D. G. d'Enterria, G. Martínez, L. Aphecetche, H. Delagrange, F. Fernández, H. Löhner, R. Ostendorf, Y. Schutz, and H. W. Wilschut, Phys. Lett. B **538**, 27 (2002).
[19] G. Martinez, F. M. Marqués, Y. Schutz, Gy. Wolf, J. Díaz, M. Franke, S. Hlavác, R. Holzmann, P. Lautridou, F. Lefèvre, H. Löhner, A. Marín, T. Matulewicz, W. Mittig, R. W. Ostendorf, J. H. G. van Pol, J. Québert, P. Roussel-Chomaz, A. Schubert, R. H. Siemssen, R. S. Simon, Z. Sujkowski, V. Wagner, and H. W. Wilschut, Phys. Lett. B **349**, 23 (1995).
[20] D. G. d'Enterria, L. Aphecetche, A. Chbihi, H. Delagrange, J. Díaz, M. J. van Goethem, M. Hoefman, A. Kugler, H. Löhner, G. Martínez, M. J. Mora, R. Ortega, R. W. Ostendorf, S. Schadmand, Y. Schutz, R. H. Siemssen, D. Stracener, P. Tlusty, R. Turrisi, M. Volkerts, V. Wagner, H. W. Wilschut, and N. Yahlali, Phys. Rev. Lett. **87**, 022701 (2001).
[21] J. Aichelin, Phys. Rep. **202**, 233 (1991).
[22] C. Hartnack, Li Zhuxia, L. Neise, G. Peilert, A. Rosenhauer, H. Sorge, J. Aichelin, H. Stöcker, and W. Greiner, Nucl. Phys. A **495**, 303 (1989).
[23] B. A. Brown, Phys. Rev. C **58**, 220 (1998).
[24] N. Gan, K.-T. Brinkmann, A. L. Caraley, B. J. Fineman, W. J. Kernan, and R. L. McGrath, Phys. Rev. C **49**, 298 (1994).
[25] F. Zhang, C. Li, L. Zhu, H. Liu, and F. S. Zhang, Phys. Rev. C **91**, 034617 (2015).
[26] J. Su, L. Zhu, W. J. Xie, and F. S. Zhang, Phys. Rev. C **85**, 017604 (2012).
[27] G. Tian, Z. Chen, R. Han, F. Shi, F. Luo, Q. Sun, L. Song, X. Zhang, G. Q. Xiao, R. Wada, and A. Ono, Phys. Rev. C **97**, 034610 (2018).
[28] J. Richert and P. Wagner, Phys. Rep. **350**, 1 (2001).
[29] W. Bauer, Phys. Rev. Lett. **61**, 2534 (1988).
[30] J. Y. Liu, W. J. Guo, S. J. Wang, W. Zuo, Q. Zhao, and Y. F. Yang, Phys. Rev. Lett. **86**, 975 (2001).
[31] Y. Schutz, G. Martínez, F. M. Marqués, A. Marín, T. Matulewicz, R. W. Ostendorf, P. Bozek, H. Delagrange, J. Díaz, M. Franke, K. K. Gudima, S. Hiaváč, R. Holzmann, P. Lautridou, F. Lefèvre, H. Löhner, W. Mittig, M. Płoszajczak, J. H. G. van Pol, J. Québert, P. Roussel-Chomaz, A. Schubert, R. H. Siemssen, R. S. Simon, Z. Sujkowski, V. D. Toneev, V. Wagner, H. W. Wilschut, and Gy. Wolf, Nucl. Phys. A **622**, 404 (1997).
[32] R. Ortega, Czech. J. Phys. **50**, 91 (1999).